Superdeformed Λ hypernuclei with antisymmetrized molecular dynamics

M. Isaka,[1] K. Fukukawa,[2] M. Kimura,[3] E. Hiyama,[1] H. Sagawa,[1,4] and Y. Yamamoto[1]

[1]*RIKEN Nishina Center, RIKEN, Wako, Saitama 351-0198, Japan*

[2]*Instituto Nazionale di Fisica Nucleare, Sezione di Catania, Via Santa Sofia 64, I-95123 Catania, Italy*

[3]*Department of Physics, Hokkaido University, Sapporo 060-0810, Japan*

[4]*Center for Mathematics and Physics, University of Aizu, Aizu-Wakamatsu, Fukushima 965-8560, Japan*

(Received 10 January 2014; published 19 February 2014)

The response to the addition of a Λ hyperon is investigated for the deformed states such as superdeformation in ${}^{41}_{\Lambda}$Ca, ${}^{46}_{\Lambda}$Sc, and ${}^{48}_{\Lambda}$Sc. In the present study, we use the antisymmetrized molecular dynamics model. It is pointed out that many kinds of deformed bands appear in ^{45}Sc and ^{47}Sc. Especially, it is found that there exists superdeformed states in ^{45}Sc. By the addition of a Λ particle to ^{40}Ca, ^{45}Sc, and ^{47}Sc, it is predicted, for the first time, that the superdeformed states exist in the hypernuclei ${}^{41}_{\Lambda}$Ca and ${}^{46}_{\Lambda}$Sc. The manifestation of the dependence of the Λ-separation energy on nuclear deformation such as spherical, normal deformation, and superdeformation is shown in the energy spectra of ${}^{41}_{\Lambda}$Ca, ${}^{46}_{\Lambda}$Sc, and ${}^{48}_{\Lambda}$Sc hypernuclei.

DOI: 10.1103/PhysRevC.89.024310 PACS number(s): 21.80.+a, 02.70.Ns, 27.40.+z

I. INTRODUCTION

One of the main purposes to study the structure of hypernuclei is to investigate nuclear responses when a Λ particle is added to the nucleus. Since a Λ hyperon is free from the nuclear Pauli principle, we have many interesting phenomena in hypernuclei. For example, in light p-shell hypernuclei with $A \leqslant 10$, it was pointed out that the Λ participation gives rise to more bound states and the appreciable contraction of the system (this stabilization is called the "gluelike" role of the Λ particle) by the cluster model [1–3]. In heavier p-shell ($A \geqslant 10$) and sd-shell Λ hypernuclei, there is a huge variety of nuclear structure, because they have both α-clustering and (compacting and/or deformed) shell-model-like structures. For example, in ${}^{13}_{\Lambda}$C, we found the dynamical contraction of the clustering states as much as 30% by addition of a Λ hyperon, while in the compacting shell-model-like state, there was almost no dynamical shrinkage [4,5].

It is also interesting to investigate the difference of the Λ-separation energy (B_Λ) between the cluster and shell-model-like states. For example, in ${}^{13}_{\Lambda}$C, it is found that the B_Λ is smaller in the clustering state than in the compacting shell-model-like states by more than 3 MeV [4]. In ${}^{20}_{\Lambda}$Ne, it is predicted that the B_Λ is larger in the shell-model-like ground state than in the negative-parity cluster state [6]. However, this result is different from the cluster model calculation [7]. Therefore it is important to reveal differences of B_Λ depending on the structures.

Let us consider the heavier nuclei with $20 \leqslant A \leqslant 40$. It is of interest to investigate nuclear response when a Λ particle is injected into such heavier nuclei. In these nuclei, there are various interesting phenomena such as the coexistence of spherical, normal-deformed (ND), and clustering states in the low-lying energy regions. Therefore it is expected that a Λ particle generates the hypernuclear states with various structures and modifies them. For example, it is pointed out that the shrinking effect of α-clustering states will appear by adding a Λ particle [8,9]. It is predicted that the shape of ${}^{29}_{\Lambda}$Si is changed to be spherical by a Λ particle, whereas the corresponding core nucleus ^{28}Si is oblately deformed [10].

It is interesting to study structure of Sc isotopes, because of the coexistence of spherical and normal-deformed states. Many authors studied the structure of odd Sc isotopes, in which the positive-parity and negative-parity bands coexist near the ground state. This is inconsistent with the naive shell-model picture which suggests only the negative-parity states near the ground state. For example, ^{45}Sc has the degenerated positive-parity state $3/2^+$ near the ground state $(7/2^-)$ with $\Delta E = 12$ keV. In ^{47}Sc, the positive-parity state $3/2^+$ lies at only 0.77 MeV above the ground state $7/2^-$. The occurrence of the low-lying positive-parity states can be explained as a proton 2-particle 1-hole ($2p$-$1h$) state in the Nilsson model [11–14]. In other words, it could be said that the low-lying positive-parity states are deformed, while the ground states $7/2^-$ are almost spherical. By adding a Λ hyperon to them, it is expected that the low-lying excitation spectra will be modified in Sc Λ hypernuclei, because the B_Λ will be different depending on the deformation. Especially, in the case of the hyperon in the s wave, it is predicted that the Λ-separation energy B_Λ becomes larger for the spherical state than the deformed state [6,10,15–17]. Therefore, the addition of a Λ particle will affect the low-lying spectra of Sc isotopes, and hence we expect that Sc isotopes are suited to verify the dependence of B_Λ on nuclear deformation, which is one of the purposes of this study.

Another interesting issue in Λ hypernuclei with $A \sim 40$ is to study the low-lying states with very large deformation, i.e., superdeformed (SD) states. It is considered that the SD state is related with the appearance of large shell gaps at a 2 : 1 axis ratio of the nuclear deformation for specific particle numbers. Recently, many SD bands are investigated and identified in nuclei with $A \sim 40$ [18–20]. For example, in ^{40}Ca, a SD band is confirmed by the observation of the $K^\pi = 0^+$ band built on the 0^+_3 state lying at 5.21 MeV, while its ground state is spherical due to the double closed-shell structure [19,21]. It is expected that in some Sc isotopes, the SD states will appear in the low-lying regions, which could be accessed by the ^{24}Mg $+{}^{24}$ Mg reaction fusion-evaporation experiment at the Grand Accélérateur National d'Ions Lourds (GANIL) [22].

 ©2014 American Physical Society

The second purpose of the present study is the difference of B_Λ which indicates a difference of deformations. To investigate it, we perform antisymmetrized molecular dynamics (AMD) calculations for ^{40}Ca, ^{45}Sc, and ^{47}Sc and the corresponding Λ hypernuclei. The AMD model was applied successfully to several normal nuclei with $A \sim 40$ such as ^{40}Ca [23,24] to reveal the structure of the SD states without assumptions on nuclear deformations and clustering. In this study, we apply the same AMD framework as done in Ref. [24] so as to predict the existence of the ND and SD bands in ^{45}Sc and ^{47}Sc. In the hypernuclear study, an extended version of the AMD model for hypernuclei (HyperAMD) is applied to investigate the hypernuclear SD states. It was known that the HyperAMD succeeded in describing the low-lying structure of p- and sd-shell Λ hypernuclei combined with the generator coordinate method (GCM) [9]. Thus the HyperAMD is confirmed as a powerful tool to study the structure of the Λ hypernuclei with $A \sim 40$ having various deformations. It is very important to use a reliable ΛN interaction for calculations of B_Λ values. We adopt here the ΛN G-matrix interaction derived from the extended soft-core (ESC) model [25], which reproduces B_Λ values of Λ hypernuclei systematically [26]. The present study is very much motivated by an experimental project at the Thomas Jefferson National Accelerator Facility (JLab) which is planned to produce from s shell with $A \sim 4$ up to $A \sim 208\Lambda$ hypernuclei by the $(e,e'K^+)$ reaction. There is high expectation to observe the SD states in $^{46}_{\Lambda}$Sc and $^{48}_{\Lambda}$Sc by the ^{46}Ti (^{48}Ti) $(e,e'K^+)$ at JLab.

This paper is organized as follows: In the next section, we explain the theoretical framework of HyperAMD. In Sec. III, the changes of the Λ single-particle energy as a function of quadrupole deformation are presented. The difference of the Λ-separation energy in $^{41}_{\Lambda}$Ca among the ground ND and SD states is also discussed in this section. In Sec. IV, the existence of the hypernuclear SD states and the changes of the excitation spectra are discussed for $^{46}_{\Lambda}$Sc and $^{48}_{\Lambda}$Sc. The final section summarizes this work.

II. FRAMEWORK

In this study, we apply the HyperAMD combined with the generator coordinate method (GCM) [9] to $^{41}_{\Lambda}$Ca, $^{46}_{\Lambda}$Sc, and $^{48}_{\Lambda}$Sc hypernuclei.

A. Hamiltonian and variational wave function

The Hamiltonian used in this study is given as

$$\hat{H} = \hat{H}_N + \hat{H}_\Lambda - \hat{T}_g, \tag{1}$$

$$\hat{H}_N = \hat{T}_N + \hat{V}_{NN} + \hat{V}_{\rm Coul}, \tag{2}$$

$$\hat{H}_\Lambda = \hat{T}_\Lambda + \hat{V}_{\Lambda N}. \tag{3}$$

Here, $\hat{T}_N$, $\hat{T}_\Lambda$, and $\hat{T}_g$ are the kinetic energies of nucleons, a Λ hyperon, and the center-of-mass motion, respectively. We use the Gogny D1S interaction [27] as an effective nucleon-nucleon interaction $\hat{V}_{NN}$. In ^{45}Sc and ^{47}Sc, we tune the spin-orbit interaction of Gogny D1S to reproduce the observed excitation energy of the $3/2^+_1$ state of ^{45}Sc. The Coulomb interaction $\hat{V}_{\rm Coul}$ is approximated by the sum of seven Gaussians. We use the G-matrix interaction as a ΛN effective interaction $\hat{V}_{\Lambda N}$.

The intrinsic wave function of a single Λ hypernucleus composed of a core nucleus with mass A and a Λ hyperon is described by the parity-projected wave function, $\Psi^\pi = \hat{P}^\pi \Psi_{\rm int}$, where $\hat{P}^\pi$ is the parity projector and $\Psi_{\rm int}$ is the intrinsic wave function given as

$$\Psi_{\rm int} = \Psi_N \otimes \varphi_\Lambda, \quad \Psi_N = \frac{1}{\sqrt{A!}} \det\{\phi_i(r_j)\}, \tag{4}$$

$$\phi_i = \prod_{\sigma=x,y,z} \left(\frac{2\nu_\sigma}{\pi}\right)^{\frac{1}{4}} \exp\left\{-\nu_\sigma (r - Z_i)^2_\sigma\right\} \chi_i \eta_i, \tag{5}$$

$$\varphi_\Lambda = \sum_{m=1}^{M} c_m \chi_m \prod_{\sigma=x,y,z} \left(\frac{2\nu_\sigma}{\pi}\right)^{\frac{1}{4}} e^{-\nu_\sigma (r - z_m)^2_\sigma}, \tag{6}$$

$$\chi_i = \alpha_i \chi_\uparrow + \beta_i \chi_\downarrow, \quad \chi_m = a_m \chi_\uparrow + b_m \chi_\downarrow, \tag{7}$$

$$\eta_i = \text{proton or neutron}, \tag{8}$$

where ϕ_i is the ith nucleon single-particle wave packet consisting of spatial, spin χ_i, and isospin η_i parts. The variational parameters are the centroids of Gaussian $\boldsymbol{Z}_i$ and z_m, width parameters ν_σ, spin directions α_i, β_i, α_m, and β_m, and coefficients c_m. We approximately remove the spurious center-of-mass kinetic energy in the same way as Ref. [6].

B. Variation with constraint on nuclear quadrupole deformation β

The energy variation is performed under the constraint on nuclear matter quadrupole deformation parameter β in the same way as our previous works [6,9]. By the frictional cooling method, the variational parameters in Ψ^π for the Λ hypernucleus and Ψ^π_N for the core nucleus are determined for each β, and the resulting wave functions are denoted $\Psi^\pi(\beta)$ and $\Psi^\pi_N(\beta)$, respectively. It is noted that the nuclear quadrupole deformation parameter γ is optimized through the energy variation for each β. By using the wave functions $\Psi^\pi(\beta)$ and $\Psi^\pi_N(\beta)$, we calculate the parity-projected intrinsic energies defined as

$$E^\pi_{hyp}(\beta) = \left\langle \Psi^\pi(\beta) \middle| \hat{H} \middle| \Psi^\pi(\beta) \right\rangle / \langle \Psi^\pi(\beta) | \Psi^\pi(\beta) \rangle, \tag{9}$$

$$E^\pi_{\rm cor}(\beta) = \left\langle \Psi^\pi_N(\beta) \middle| \hat{H} \middle| \Psi^\pi_N(\beta) \right\rangle / \langle \Psi^\pi_N(\beta) | \Psi^\pi_N(\beta) \rangle, \tag{10}$$

for the Λ hypernucleus and the core nucleus, respectively.

It is found that the Λ hyperon dominantly occupies an s wave in the hypernuclear states, because no constraint is imposed on the Λ single-particle wave function in the present calculation. Combined with the parity projection, we obtained two kinds of configurations in which the Λ hyperon couples to the positive- and negative-parity states of the core. Here

these two are denoted $\Psi_N^+ \otimes \Lambda$ and $\Psi_N^- \otimes \Lambda$, respectively, in the following discussions.

C. Angular-momentum projection and generator coordinate method

After the variational calculation, we project out an eigenstate of the total angular momentum from the hypernuclear states,

$$\Psi_{MK}^{J\pi}(\beta_i) = \frac{2J+1}{8\pi^2} \int d\Omega D_{MK}^{J*}(\Omega) \hat{R}(\Omega) \Psi^{\pi}(\beta_i). \quad (11)$$

The integrals are performed numerically over three Euler angles Ω.

The wave functions $\Psi_{MK}^{J\pi}(\beta_i)$ which have the same parity and angular momentum but have different K and nuclear quadrupole deformation β_i are superposed (GCM). Then the wave function of the system is written as

$$\Psi_{\alpha}^{J\pi} = c_{\alpha} \Psi_{MK}^{J\pi}(\beta) + c'_{\alpha} \Psi_{MK'}^{J\pi}(\beta') + \cdots, \quad (12)$$

where the quantum numbers except for the total angular momentum and the parity are represented by α. The coefficients $c_{\alpha}, c'_{\alpha}, \ldots$ are determined by the Hill–Wheeler equation.

D. Analysis of wave function

It is convenient to define the Λ single-particle energy ϵ_{Λ} as

$$\epsilon_{\Lambda}(\beta) = \left\langle \Psi^{\pi}(\beta) \left| \hat{H}_{\Lambda} \right| \Psi^{\pi}(\beta) \right\rangle / \langle \Psi^{\pi}(\beta) | \Psi^{\pi}(\beta) \rangle \quad (13)$$

to discuss how the Λ binding energy changes for increasing the nuclear deformation.

We also calculate the energy gain B_{Λ} of each state J^{π} in a hypernucleus from the corresponding state of the core nucleus as follows:

$$B_{\Lambda} = E\left({}^{A}\mathrm{Z}(j^{\pi})\right) - E\left({}^{A+1}_{\Lambda}\mathrm{Z}(J^{\pi})\right). \quad (14)$$

Here, $E({}^{A}\mathrm{Z}(j^{\pi}))$ and $E({}^{A+1}_{\Lambda}\mathrm{Z}(J^{\pi}))$ respectively represent the total energies of the j^{π} state of the core nuclei and the corresponding J^{π} state of the hypernuclei. B_{Λ} shows the Λ-separation energy for each state of hypernuclei.

To analyze the nucleon configurations for the wave functions on energy curves, we calculate the number of the deformed harmonic oscillator quanta for protons (N^p) and neutrons (N^n) in the same way as Refs. [28,29]. The number operators are defined as

$$\hat{N}^{p(n)} = \sum_i \sum_{\sigma=x,y,z} \left(\frac{p_{\sigma i}^2}{4\hbar^2 \nu_{\sigma}} + \nu_{\sigma} r_{\sigma i}^2 - \frac{3}{2} \right), \quad (15)$$

where summation over i runs all protons (neutrons) [28]. Here the expectation values of $\hat{N}^{\xi}$, $N^{\xi} = \langle \Psi_N^{\pi} | \hat{N}^{\xi} | \Psi_N^{\pi} \rangle / \langle \Psi_N^{\pi} | \Psi_N^{\pi} \rangle$ are calculated for the parity-projected states of the core nuclei.

We introduce the overlap between the GCM wave function $\Psi_{\alpha}^{J\pi}$ and $\Psi_{MK}^{J\pi}(\beta)$,

$$O_{MK\alpha}^{J\pi}(\beta) = \left| \left\langle \Psi_{MK}^{J\pi}(\beta) \middle| \Psi_{\alpha}^{J\pi} \right\rangle \right|^2. \quad (16)$$

Since the GCM overlap $O_{MK\alpha}^{J\pi}(\beta)$ shows the contributions from $\Psi_{MK}^{J\pi}(\beta)$ to each state J^{π}, it is useful to estimate the nuclear quadrupole deformation β of each state. Namely, we regard β corresponding to the maximum GCM overlap as the nuclear deformation of each state. We call the deformed states with $\beta < 0.5$ ND, and those with $\beta \geqslant 0.5$ SD. Detailed discussions about ND and SD will be performed in the next section.

E. ΛN effective interaction

It is reasonable to use an effective ΛN interaction in our model where short-range and tensor correlations are not included. The G-matrix theory makes it possible to derive a realistic effective interaction in a model space, starting from a free-space interaction. Baryon-baryon interaction models of the SU(3) flavor-octet baryons have been developed with use of YN scattering data and also hypernuclear information. One of them is the extended-soft-core (ESC) model [25] by the Nijmegen group, and the latest version is called ESC08c [30]. Almost all hypernuclear data are reproduced consistently by ESC08c. In this study, we use the YN G-matrix interaction (YNG) derived from ESC08c. The YNG is obtained in nuclear matter and represented in a three-range Gaussian form:

$$G(r; k_F) = \sum_{i=1}^{3} \left(a_i + b_i k_F + c_i k_F^2 \right) \exp\left(-r^2/\beta_i^2 \right). \quad (17)$$

Here, an interaction strength in each ΛN state depends on a nuclear Fermi momentum k_F, reflecting the density-dependence of the G matrix in nuclear medium. It should be noted that the ΛN-ΣN coupling term included in ESC08c is renormalized into the ΛN-ΛN part of the G-matrix interaction, giving rise to the important part of the density dependence. Values of parameters (a_i, b_i, c_i) and β_i are given in the Appendix.

In the case of using the YNG interaction, decisively important is how to treat its k_F dependence in a structure calculation. In Ref. [26], the averaged-density approximation (ADA) was demonstrated to be very reliable to reproduce spectra of Λ hypernuclei with YNG interactions, where k_F values in YNG were obtained from expected values of nuclear density distributions by Λ wave functions.

According to the ADA treatment, the k_F value is calculated for each configuration of ${}^{41}_{\Lambda}$Ca, ${}^{46}_{\Lambda}$Sc, and ${}^{48}_{\Lambda}$Sc by using the wave function $\Psi^{\pi}(\beta_0)$, where β_0 corresponds to the maximum of the GCM overlap. It is found that the obtained k_F values are the same for the $\Psi_N^- \otimes \Lambda$ and $\Psi_N^+ \otimes \Lambda$ states of each Sc hypernuclei. Finally, we take $k_F = 1.26$ fm^{-1} for ${}^{41}_{\Lambda}$Ca, $k_F = 1.29$ fm^{-1} for ${}^{46}_{\Lambda}$Sc, and $k_F = 1.30$ fm^{-1} for ${}^{48}_{\Lambda}$Sc in the GCM calculations.

III. DIFFERENCE OF B_{Λ} AMONG THE SPHERICAL, NORMAL-DEFORMED, AND SUPERDEFORMED STATES IN ${}^{41}_{\Lambda}$Ca

First, we show the results of ^{40}Ca and ${}^{41}_{\Lambda}$Ca. Because there exist the ND and SD states in ^{40}Ca, it is of interest to discuss the difference of the Λ-separation energy in ${}^{41}_{\Lambda}$Ca. Here we briefly explain the properties of the deformed states of ^{40}Ca. It is observed that in ^{40}Ca there exist the ND and SD bands built on the 0_2^+ (at 3.35 MeV)

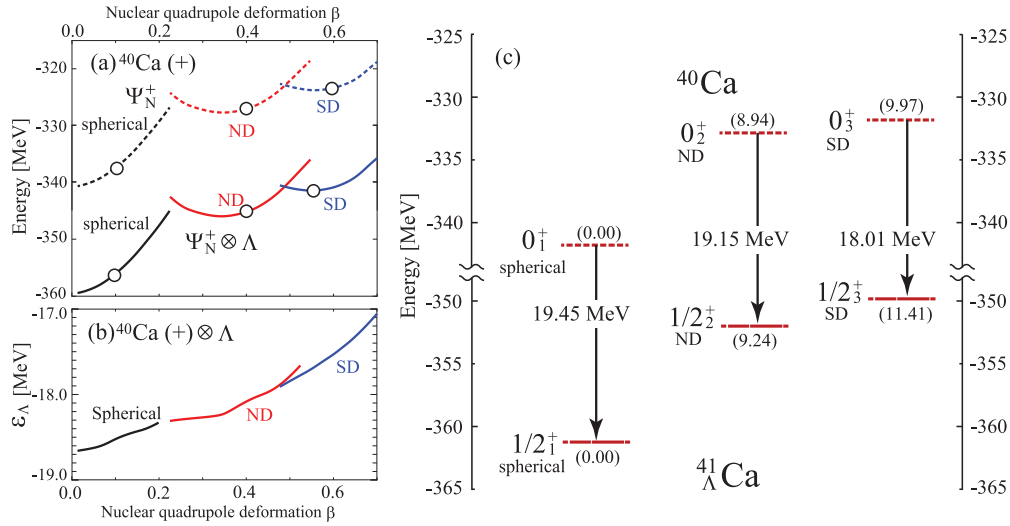

FIG. 1. (Color online) (a) Energy curves as a function of the nuclear quadrupole deformation β for ^{40}Ca (dotted) and $^{41}_{\Lambda}$Ca (solid). Deformation parameter γ is optimized through the energy variation for each β. Open circles show the deformations β of the 0^+ and $1/2^+$ states calculated by the GCM corresponding to the energy curves. (b) Λ single-particle energy defined by Eq. (13) for $^{41}_{\Lambda}$Ca. (c) Calculated energies of the 0^+ states in ^{40}Ca (dotted) and $1/2^+$ states in $^{41}_{\Lambda}$Ca (solid). The values in parentheses are the calculated excitation energies from the ground states of ^{40}Ca and $^{41}_{\Lambda}$Ca in MeV, respectively.

and 0^+_3 (5.21 MeV) states, respectively [19,21]. The SD band is considered to have the $[(sd)^{-4}(pf)^4]_\pi[(sd)^{-4}(pf)^4]_\nu$ configuration, while the configuration of the ND band is $[(sd)^{-2}(pf)^2]_\pi[(sd)^{-2}(pf)^2]_\nu$ [19,31,32]. Our results for ^{40}Ca shown in Fig. 1 are identical to those reported in Ref. [24], since the same theoretical model and effective interaction are applied. The energy curve of ^{40}Ca as a function of the deformation parameter β [dotted line in Fig. 1(a)] shows the spherical-energy minimum having the sd closed-shell configuration, which corresponds to the ground state. It also shows two well-determined local energy minima at $\beta = 0.35$ and $\beta = 0.55$ which correspond to the ND and SD states of ^{40}Ca mentioned above, respectively.

Furthermore, in Fig. 1(a), we show the energy curve of $^{41}_{\Lambda}$Ca, which is similar in that of ^{40}Ca. In Fig. 1(b), the Λ single-particle energies with respect to nuclear quadrupole deformation β are illustrated. We see that the Λ single-particle energy $\epsilon_\Lambda(\beta)$ varies depending on β, i.e., ϵ_Λ has the minimum at $\beta = 0$ and becomes shallower as β increases. This means that a Λ hyperon is most deeply bound to the spherical-shape

TABLE I. Calculated excitation energy E_x in MeV, matter quadrupole deformation β and γ (deg), and rms radii (fm). The B_Λ defined by Eq. (14) is also listed in unit of MeV for $^{41}_{\Lambda}$Ca.

	J^π	E_x (MeV)	β	γ (deg)	$r_{\rm rms}$ (fm)	B_Λ
$^{41}_{\Lambda}$Ca	$1/2^+_1$	0.00	0.10	0	3.38	19.45
	$1/2^+_2$	9.24	0.40	27	3.47	19.15
	$1/2^+_3$	11.41	0.55	13	3.58	18.01
^{40}Ca	0^+_1	0.00	0.12	12	3.39	
	0^+_2	8.94	0.40	28	3.50	
	0^+_3	9.97	0.60	17	3.63	

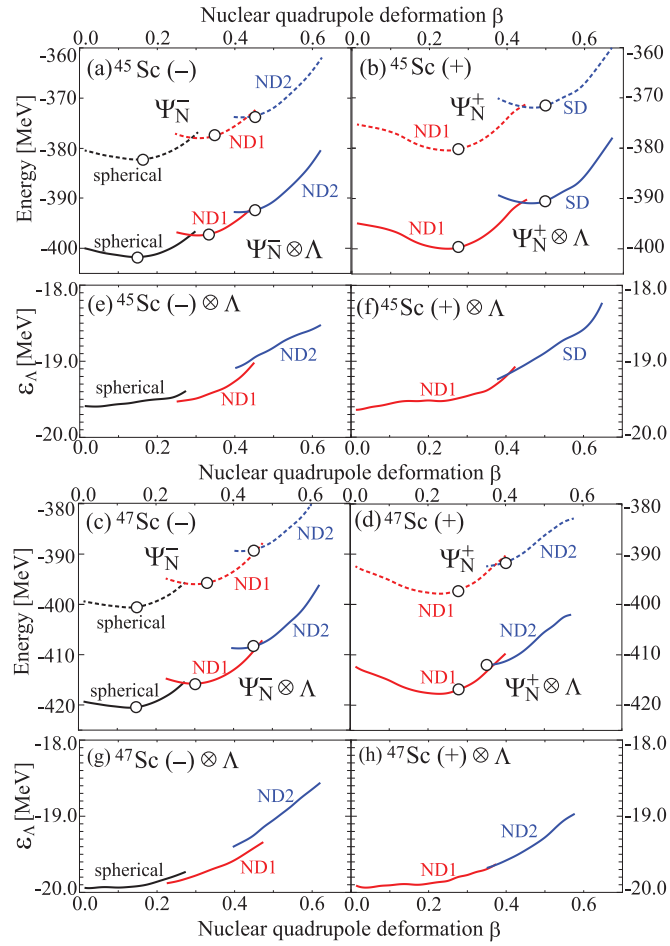

FIG. 2. (Color online) Same as Figs. 1(a) and 1(b), for ^{45}Sc and ^{47}Sc and the corresponding hypernuclei. Open circles show the deformation β of the corresponding states obtained after the GCM calculation.

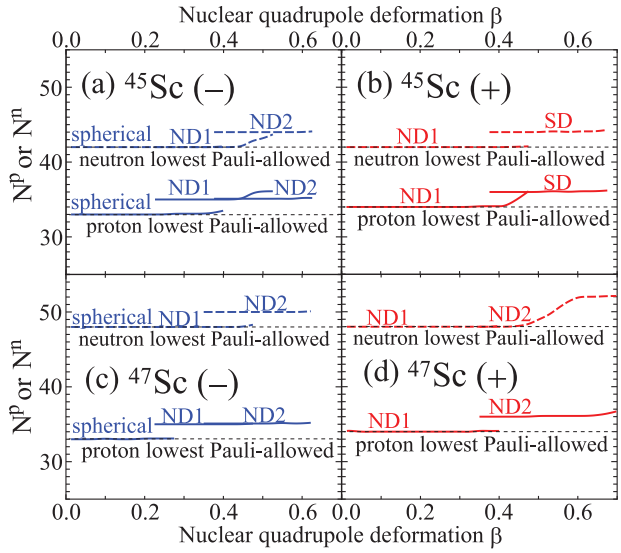

FIG. 3. (Color online) Numbers of the deformed harmonic oscillator quanta N^p (solid) and N^n (dashed), defined by Eq. (15), calculated from the wave functions on the energy curves shown in Figure 2. Panels (a) and (b) [(c) and (d)] correspond to the negative- and positive-parity states of ^{45}Sc (^{47}Sc).

core nucleus, which is consistent with the previous works for p- and sd-shell hypernuclei such as $^{13}_{\Lambda}$C and $^{21}_{\Lambda}$Ne [6,15].

The difference of ϵ_Λ will lead to the difference of B_Λ and affect the excitation spectra of Λ hypernuclei. To investigate it, we perform the GCM calculation for ^{40}Ca and $^{41}_{\Lambda}$Ca by using the wave functions on the energy curves. Figure 1(c) and Table I show the calculated energies of three $1/2^+$ states of $^{41}_{\Lambda}$Ca, in which a Λ in s orbit is coupled to the ground, ND,

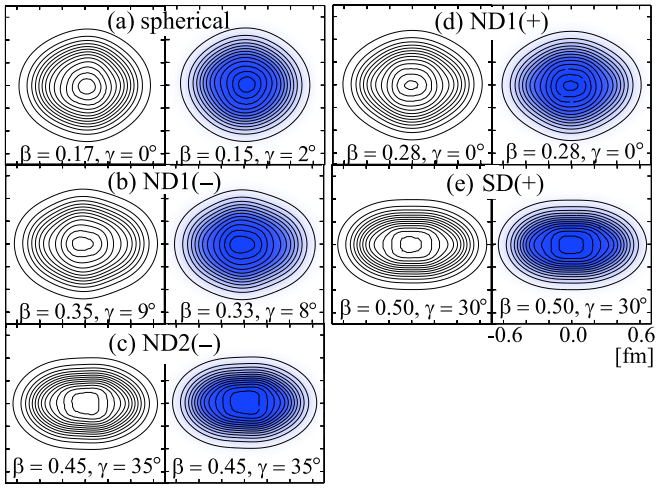

FIG. 4. (Color online) (a)–(c) Intrinsic density distributions of the negative-parity spherical, ND1, and ND2 states in ^{45}Sc and $^{46}_{\Lambda}$Sc, respectively. In each panel, contour lines show the nuclear density, while the color plots present the distribution of Λ. Values β and γ are deformations of each state determined by the GCM overlap. (d), (e) Same as panels (a)–(c) but for the positive-parity ND1 and SD states of ^{45}Sc and $^{46}_{\Lambda}$Sc.

and SD 0^+ states of ^{40}Ca. We also calculate the B_Λ, defined by Eq. (14), for each state. It is found that the Λ-separation energy for the ground state $1/2^+_1$ is $B_\Lambda = 19.45$ MeV which is consistent with the empirical formula of B_Λ [33]. The B_Λ is the largest for the spherical ground state, 19.45 MeV, and smallest for the SD $1/2^+_3$ state, 18.01 MeV. We see the energy difference about 1.4 MeV between the spherical and SD states.

Let us see the changes of radii and deformation by the Λ addition. As shown in Table I, we do not have any difference in radii and deformations for the ground and ND states. On the other hand, in the SD state, it is seen that shrinkage of the radius by about 1.4% and the reduction of nuclear quadrupole deformation.

IV. SCANDIUM HYPERNUCLEI

In odd Sc isotopes, it has been discussed, from the late 1960s, that the disappearance of the magic number $N = 20$ and the coexistence of the different deformations in the ground-state energy region, i.e., the appearance of the low-lying positive-parity states due to the promotion of a proton from the sd shell [11–14,34–37]. Furthermore, it is expected that many-particle–many-hole (mp-mh) states exist within the small excitation energy. Especially, Sc isotopes could have largely deformed states with a similar nucleon configuration to the SD states of ^{40}Ca. In this section, we focus on the response of the Λ addition to ^{45}Sc and ^{47}Sc.

A. Many-particle–many-hole and superdeformed states

In ^{45}Sc and ^{47}Sc, we calculate the energy curves as a function of β for the negative- and positive-parity states. In Figs. 2(a)–2(d), it is found that three (two) energy curves with the different minima are obtained for the negative-parity (positive-parity) state. As shown in Fig. 2(a), we obtain one spherical energy minimum and two ND minima with different deformations in the negative-parity states of ^{45}Sc and $^{46}_{\Lambda}$Sc. In Fig. 2(b), we predict the ND and SD minima as the positive-parity states of ^{45}Sc and $^{46}_{\Lambda}$Sc, while only ND minima are obtained in ^{47}Sc and $^{48}_{\Lambda}$Sc. To analyze the nucleon configuration of these energy curves, we calculate the

TABLE II. Same as Table I but for $^{46}_{\Lambda}$Sc and $^{48}_{\Lambda}$Sc and corresponding nuclei.

		J^π	E_x (MeV)	β	γ (deg)	$r_{\rm rms}$ (fm)	B_Λ (MeV)
$^{46}_{\Lambda}$Sc	spherical	4^-_1	0.00	0.15	2	3.51	19.95
	ND2	2^-_4	2.47	0.45	35	3.61	19.66
	SD	1^+_2	3.85	0.50	30	3.61	19.52
^{45}Sc	spherical	$7/2^-_1$	0.00	0.17	0	3.51	
	ND2	$3/2^-_3$	2.18	0.45	35	3.62	
	SD	$3/2^+_2$	3.41	0.50	30	3.64	
$^{48}_{\Lambda}$Sc	spherical	4^-_1	0.00	0.15	8	3.53	20.12
	ND2	3^-_5	5.98	0.45	59	3.63	19.69
	ND2	0^+_1	3.96	0.35	15	3.59	19.88
^{47}Sc	spherical	$7/2^-_1$	0.00	0.15	8	3.54	
	ND2	$5/2^-_3$	5.55	0.45	59	3.65	
	ND2	$1/2^+_1$	3.72	0.40	17	3.63	

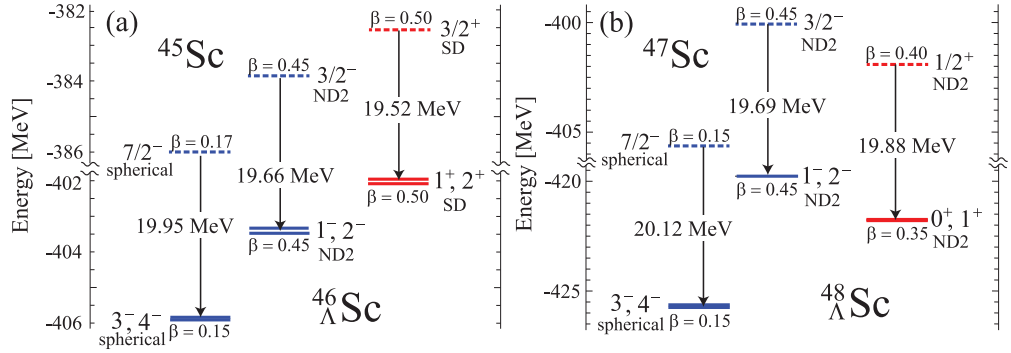

FIG. 5. (Color online) (a) Calculated energies of the ground and deformed states corresponding to the spherical, ND2, and SD minima of ^{45}Sc and $^{46}_{\Lambda}$Sc shown in Figs. 2(a) and 2(b). (b) Same as panel (a) but for the spherical and ND2 minima of ^{47}Sc and $^{48}_{\Lambda}$Sc shown in Figs. 2(c) and 2(d).

numbers of the deformed harmonic oscillator quanta N^p and N^n, defined by Eq. (15), using the wave functions on each energy curve. The N^p (N^n) shows the sd-shell closed and/or particle-hole configurations of the protons (neutrons). In Fig. 3, it is found that the wave functions on each energy curve have the same nucleon configuration. Since the lowest value allowed by the Pauli principle is $N^p = 33$ and $N^n = 42$ ($N^p = 33$ and $N^n = 48$) for ^{45}Sc (^{47}Sc), the spherical minimum of ^{45}Sc (^{47}Sc) should have the $[(pf)^1]_\pi[(pf)^4]_\nu$ ($[(pf)^1]_\pi[(pf)^6]_\nu$) configuration. In Fig. 3, we see that the N^p and/or N^n values of the other curves, ND1, ND2, and SD, in ^{45}Sc and ^{47}Sc are different from the Pauli-allowed values, which indicates that these energy curves have mp-mh configurations. Among them, the energy curve denoted as SD in Fig. 2(b) is considered to have the $[(sd)^{-3}(pf)^4]_\pi[(sd)^{-2}(pf)^6]_\nu$ configuration, in which the proton configuration is similar to that of the SD states in ^{40}Ca. Furthermore, to see the deformation of ND1, ND2, and SD in ^{45}Sc visually, we illustrate the density distributions of them in Fig. 4. We see the large quadrupole deformation as β increases. By the addition of a Λ particle to these states, it is expected that the Λ-separation energy B_Λ is different depending on the deformations as discussed for $^{41}_{\Lambda}$Ca.

Next, we calculate the energy curves of $^{46}_{\Lambda}$Sc and $^{48}_{\Lambda}$Sc, and the Λ single-particle energy ϵ_Λ as function of β. The solid curves in Figs. 2(a)–2(d) show that the Λ hyperon generates the energy curves of $^{46}_{\Lambda}$Sc and $^{48}_{\Lambda}$Sc corresponding to the core nuclei. Figures 2(e)–2(h) show the ϵ_Λ as a function of β for the negative- and positive-parity states of $^{46}_{\Lambda}$Sc and $^{48}_{\Lambda}$Sc, and it is found that the behavior of $\epsilon_\Lambda(\beta)$ is quite similar to that in $^{41}_{\Lambda}$Ca.

To discuss the difference of the Λ-separation energy B_Λ, we perform the GCM calculation for ^{45}Sc and ^{47}Sc and the corresponding hypernuclei. Here we focus on the ground, SD, and largely deformed ND states, which correspond to the spherical, SD, and ND2 minima shown in Figs. 2(a)–2(d), respectively. Figure 5 and Table II show the B_Λ of the spherical and deformed states of $^{46}_{\Lambda}$Sc and $^{48}_{\Lambda}$Sc. In Fig. 5 and Table II, it is found that B_Λ is the largest in the spherical states in $^{46}_{\Lambda}$Sc and $^{48}_{\Lambda}$Sc. And it is also found that B_Λ becomes smaller as the nuclear quadrupole deformation β is increased. This trend of B_Λ is consistent with the behavior of $\epsilon_\Lambda(\beta)$ shown

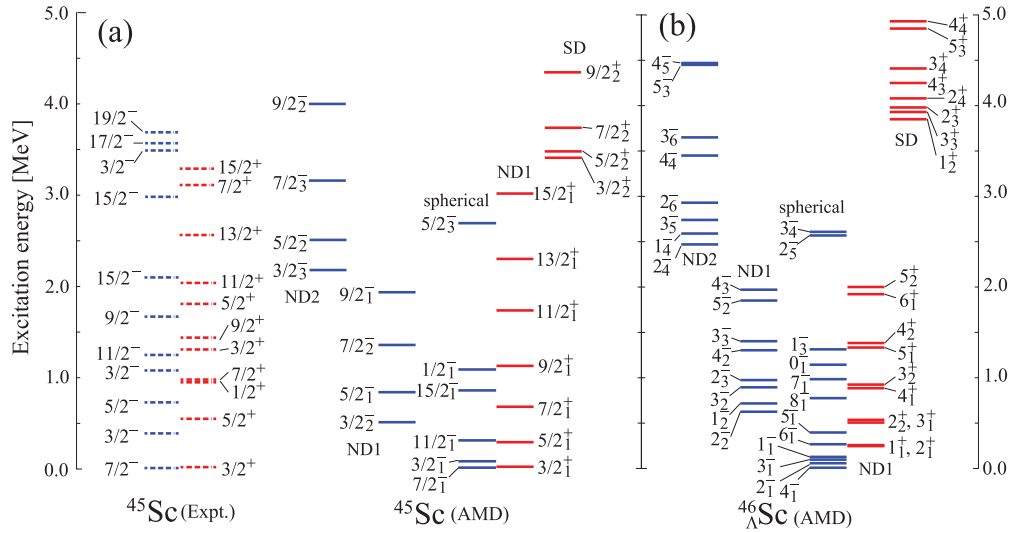

FIG. 6. (Color online) Calculated excitation spectra of ^{45}Sc and $^{46}_{\Lambda}$Sc.

TABLE III. Calculated $B(E2)$ (e^2 fm^4) values for ^{45}Sc and ^{47}Sc. Values in parentheses are observed data.

^{45}Sc			^{47}Sc		
J_i	J_f	$B(E2)$	J_i	J_f	$B(E2)$
Spherical			Spherical		
$11/2^-_1$	$7/2^-_1$	56 (108 [38])	$11/2^-_1$	$7/2^-_1$	37
$15/2^-_1$	$11/2^-_1$	33 (<818 [38])	$3/2^-_1$	$7/2^-_1$	87
$3/2^-_1$	$7/2^-_1$	132	$5/2^-_2$	$3/2^-_1$	6
$1/2^-_1$	$3/2^-_1$	111	$5/2^-_2$	$7/2^-_1$	1
$5/2^-_3$	$1/2^-_1$	69	$9/2^-_1$	$5/2^-_2$	7
$5/2^-_3$	$3/2^-_1$	20	$9/2^-_1$	$7/2^-_1$	7
ND1(−)			ND1(−)		
$5/2^-_1$	$3/2^-_2$	558	$5/2^-_1$	$3/2^-_2$	319
$7/2^-_2$	$3/2^-_2$	218	$7/2^-_2$	$3/2^-_2$	263
$7/2^-_2$	$5/2^-_1$	325	$7/2^-_2$	$5/2^-_1$	238
$9/2^-_1$	$5/2^-_1$	331	$9/2^-_2$	$5/2^-_1$	204
$9/2^-_1$	$7/2^-_2$	203	$9/2^-_2$	$7/2^-_2$	52
ND2(−)			ND2(−)		
$5/2^-_2$	$3/2^-_3$	263	$7/2^-_3$	$5/2^-_3$	542
$7/2^-_3$	$3/2^-_3$	34	$9/2^-_3$	$5/2^-_3$	153
$7/2^-_3$	$5/2^-_2$	172	$9/2^-_3$	$7/2^-_3$	457
$9/2^-_2$	$5/2^-_2$	120	$11/2^-_2$	$7/2^-_3$	259
$9/2^-_2$	$7/2^-_3$	230	$11/2^-_2$	$9/2^-_3$	350
$11/2^-_2$	$7/2^-_3$	61			
$11/2^-_2$	$9/2^-_2$	36			
$13/2^-_1$	$9/2^-_2$	19			
$13/2^-_1$	$11/2^-_2$	126			
ND1(+)			ND1(+)		
$5/2^+_1$	$3/2^+_1$	320 (360^{+332}_{-180}[13])	$5/2^+_1$	$3/2^+_1$	237 (432^{+570}_{-293}[13])
$7/2^+_1$	$3/2^+_1$	133 (62 [38])	$7/2^+_1$	$3/2^+_1$	136 (111^{+81}_{-58}[13])
$7/2^+_1$	$5/2^+_1$	199 (115^{+251}_{-91}[13])	$7/2^+_1$	$5/2^+_1$	156
$9/2^+_1$	$5/2^+_1$	185 (179 [38])	$9/2^+_1$	$5/2^+_1$	159
$9/2^+_1$	$7/2^+_1$	118 (57^{+65}_{-35}[13])	$9/2^+_1$	$7/2^+_1$	52
			ND2(+)		
$11/2^+_1$	$7/2^+_1$	214 (216 [38])	$3/2^+_2$	$1/2^+_1$	493
$11/2^+_1$	$9/2^+_1$	84	$5/2^+_2$	$1/2^+_1$	515
$13/2^+_1$	$9/2^+_1$	205 (151 [38])	$5/2^+_2$	$3/2^+_2$	192
$13/2^+_1$	$11/2^+_1$	50	$7/2^+_2$	$3/2^+_2$	639
$15/2^+_1$	$11/2^+_1$	208 (223 [38])	$7/2^+_2$	$5/2^+_2$	61
$15/2^+_1$	$13/2^+_1$	42	$9/2^+_2$	$5/2^+_2$	772
SD(+)			$9/2^+_2$	$7/2^+_2$	92
$5/2^+_2$	$3/2^+_2$	545	$11/2^+_1$	$7/2^+_2$	704
$7/2^+_2$	$3/2^+_2$	547	$11/2^+_1$	$9/2^+_2$	16
$7/2^+_2$	$5/2^+_2$	55			
$9/2^+_2$	$5/2^+_2$	835			
$9/2^+_2$	$7/2^+_2$	268			
$11/2^+_2$	$7/2^+_2$	749			

in Figs. 2(e)–2(h), and is quite similar to the $^{41}_{\Lambda}$Ca shown in Fig. 1.

Let us discuss the changes of matter radii and nuclear deformations by adding a Λ hyperon. In Table II, we see the almost no change of the matter rms radius and the nuclear quadrupole deformation β of each state by adding a Λ hyperon. Hence, a Λ hyperon does not change the radius and deformations of nuclear part significantly in $^{46}_{\Lambda}$Sc and $^{48}_{\Lambda}$Sc.

TABLE IV. The electric quadrupole moment (Q in units of e fm^2) of the $7/2^-$ and $3/2^+$ states in ^{45}Sc and ^{47}Sc. The values in parentheses are the observed data.

^{45}Sc		^{47}Sc	
J^π	Q	J^π	Q
$7/2^-$	−15 ($-22.0^{-0.2}_{-0.2}$ [39])	$7/2^-$	−13 (-22^{+3}_{-3} [39])
$3/2^+$	+18 ($+28^{+5}_{-5}$ [40])	$3/2^+$	+16

B. Excitation spectra

We discuss the excitation spectra of ^{45}Sc and ^{47}Sc and the corresponding hypernuclei, which are shown in Figs. 6 and 7. It is noted that all states shown in Figs. 6 and 7 are bound, because the lowest threshold energies of ^{45}Sc and ^{47}Sc are 6.9 MeV (^{44}Ca + p) and 8.5 MeV (^{46}Ca + p), respectively. Corresponding to ^{45}Sc (^{47}Sc), the lowest threshold of $^{46}_{\Lambda}$Sc ($^{48}_{\Lambda}$Sc) is $^{45}_{\Lambda}$Ca + p ($^{47}_{\Lambda}$Ca + p) and the threshold energy is expected to be higher than 6.9 MeV (8.5 MeV) in $^{46}_{\Lambda}$Sc ($^{48}_{\Lambda}$Sc). In ^{45}Sc and ^{47}Sc, by the GCM calculation, we obtain many excited states as shown in Figs. 6(a) and 7(a). By the GCM-overlap analysis, the negative- and positive-parity states of ^{45}Sc and ^{47}Sc are assigned as spherical, ND1, ND2, and SD states, depending on the major components of the wave function in the curves in Figs. 2(a)–2(d). For example, in ^{45}Sc, the states denoted as spherical in Fig. 6(a) are dominantly generated by the wave functions on the spherical minimum shown in Fig. 2(a). Similarly, the ND1 minimum shown in Fig. 2(a) dominantly contributes the positive-parity ND1 states in Fig. 6(a). Corresponding to the SD curve, the SD states appear in ^{45}Sc. In Table III, it is found that the ND1, ND2, and SD states in each nucleus are connected by the large $B(E2)$ values, which is a clear sign of the existence of the rotational bands. In ^{45}Sc, it is expected that the existence of the SD and ND bands can be confirmed by the observations of the inter- and intraband transitions such as $B(E2)$ through the ^{24}Mg + ^{24}Mg fusion-evaporation reaction experiment [22].

Figure 6(b) shows the calculated excitation spectra of $^{46}_{\Lambda}$Sc. It shows that the ground and excited states of $^{46}_{\Lambda}$Sc with a Λ hyperon are obtained corresponding to the spherical, ND1, ND2, and SD states of ^{45}Sc. Focusing on the SD states of $^{46}_{\Lambda}$Sc, it is found from Fig. 6 and Table II that the SD states are shifted up by about 440 keV. We see the similar shift up of the other deformed states. For example, the $3/2^-_3$ (ND2) state of ^{45}Sc with $\beta = 0.45$ is shifted up in $^{46}_{\Lambda}$Sc by about 290 keV. These shifts reflect the difference of B_Λ shown in the left panel of Fig. 5.

In $^{48}_{\Lambda}$Sc, we predict the existence of the ND1 and ND2 states with various deformations. It is found, from Fig. 7(b) and Table II, that the addition of a Λ hyperon causes the similar modification of the excitation spectra as $^{46}_{\Lambda}$Sc, in which the Λ hyperon shifts the largely deformed states up. For example, Table II shows that the excitation energy of the $5/2^-_3$ with $\beta = 0.45$ is shifted up by 430 keV in $^{48}_{\Lambda}$Sc. In this way, we find that the shifted energy is larger as β increases.

C. Response to $7/2^-$ and $3/2^+$ states by addition of Λ particle

Here, we focus on the ground and low-lying states $7/2^-_1$ and $3/2^+_1$ of ^{45}Sc. It is well known experimentally that the $3/2^+_1$

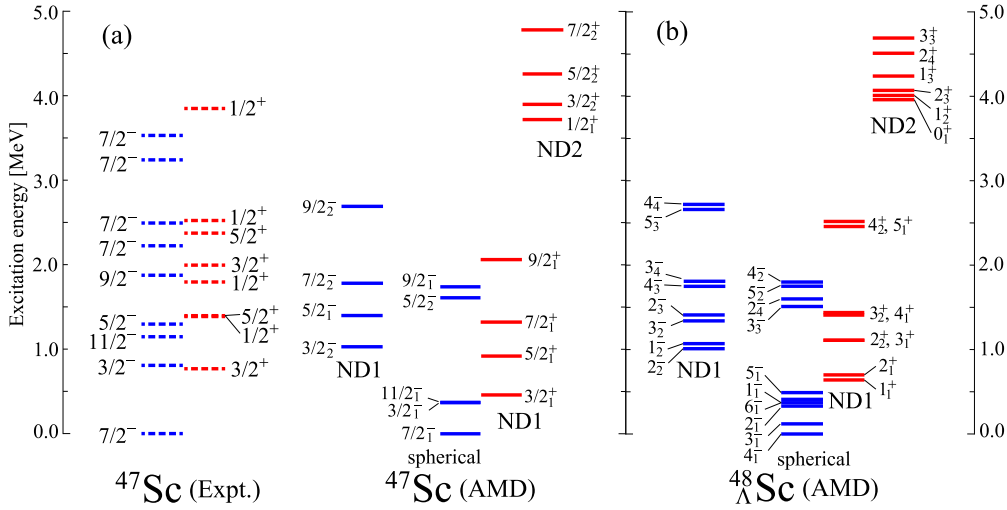

FIG. 7. (Color online) Same as Fig. 6 but for ^{47}Sc and $^{48}_{\Lambda}$Sc.

state lies slightly higher than the $7/2^-_1$ state and the energy difference between them is 12 keV. This is inconsistent with the shell-model picture, in which a $3/2^+$ state should be located at a few MeV with respect to the ground state $7/2^-_1$. This inconsistency has been extensively discussed theoretically. Then, we understand in terms of deformation by the Nilsson model as follows [11–14]: as increasing deformation, the Nilsson $K^\pi = 3/2^+$ state from the $d_{3/2}$ becomes close to the $K^\pi = 1/2^-$ state from the $0f_{7/2}$. As a result, the $3/2^+$ state becomes lower and very close to the ground state $7/2^-$. We found that deformation in the $3/2^+_1$ state is larger than that in the $7/2^-_1$ state. The calculated quadrupole deformations of $7/2^-_1$ and $3/2^+_1$ are $\beta = 0.17$ and $\beta = 0.27$, respectively. The difference of the deformations between them is also seen in the Q momentum and $B(E2)$ strength. The calculated Q momenta of the $7/2^-_1$ and $3/2^+_1$ states are listed in Table IV and are not inconsistent with the observed data within the error bars.

It is expected that the responses to Λ participation in the $7/2^-_1$ and $3/2^+_1$ states are different due to the difference in their deformations. In $^{46}_{\Lambda}$Sc, calculated B_Λ in the 1^+_1 and 2^+_1 states is 19.71 MeV, while B_Λ in the 3^-_1 and 4^-_1 states is 19.95 MeV, since the Λ-separation energy B_Λ in more-deformed states is smaller than that in less-deformed states. As a result, as shown in Fig. 8(a), the 1^+_1 and 2^+_1 states are shifted up with respect to the 3^-_1 and 4^-_1 states and the energy difference is much larger by ∼0.2 MeV. The same behavior is seen in ^{47}Sc and $^{48}_{\Lambda}$Sc [see Fig. 8(b)], and the increase of the excitation energies is also around 0.2 MeV. In Fig. 8, we see energy splitting for the ground-state doublet, 3^-_1-4^-_1, and for the excited doublet, 1^+_1-2^+_1, are quite different from each other. The reason is as follows: The number of protons in the highest orbit (pf shell) in the $7/2^-_1$ state is one, while that in the $3/2^+_1$ state is two. The energy splitting in the $7/2^-_1$ state comes from the spin-spin term in the ΛN interaction between one proton and Λ in a $0s$ orbit. If we use an even-state spin-spin term for 3^-_1-4^-_1 state, the ground states of $^{46}_{\Lambda}$Sc and $^{48}_{\Lambda}$Sc is 3^-. When we use the odd-state spin-spin term, due to the attraction of the triplet state than the singlet state, 4^- becomes the ground state. As a result, the energy splitting for the $4^-_1 - 3^-_1$ doublet is about 90 keV. On the other hand, the spin of two protons in the $3/2^+_1$ state is 0 (spin antiparallel). Then, the spin-spin part is almost canceled out and the energy splitting for the $1^+_1 - 2^+_1$ double state is negligibly small.

If we could observe these energy differences experimentally, it would be helpful to obtain information on the ΛN spin-dependent part. However, since these two energy splittings

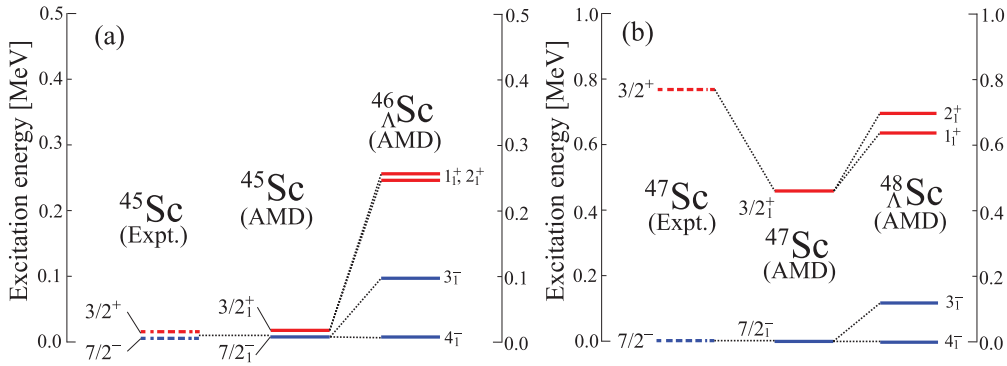

FIG. 8. (Color online) (a) The ground ($7/2^-_1$) and the lowest positive-parity states ($3/2^+_1$) of ^{45}Sc and the corresponding states in $^{46}_{\Lambda}$Sc. (b) Same as panel (a) but for ^{47}Sc and $^{48}_{\Lambda}$Sc.

TABLE V. Parameters of ΛNG-matrix interaction represented by the three range Gaussian forms given in Eq. (17) in the case of ESC08c. a_i [MeV], b_i [MeV · fm], c_i [MeV · fm^2], and β_i [fm] are given for each i.

β_i	0.5	0.9	2.0
		^1E	
a_i	−3892.0	471.5	−1.756
b_i	7401.0	−1132.0	0.0
c_i	−2821.0	446.4	0.0
		^3E	
a_i	−2135.0	229.7	−1.339
b_i	4705.0	−727.1	0.0
c_i	−1939.0	319.8	0.0
		^1O	
a_i	1785.0	103.6	−0.7956
b_i	9.656	14.47	0.0
c_i	−16.57	14.57	0.0
		^3O	
a_i	1838.0	−13.82	−1.001
b_i	−1966.0	−233.9	0.0
c_i	682.7	192.8	0.0

are less than 100 keV, they might be difficult to observe experimentally.

V. SUMMARY

We have studied the deformations of ^{40}Ca, ^{45}Sc, and ^{47}Sc, and those of the corresponding hypernuclei. For ^{45}Sc and ^{47}Sc, the deformed-basis AMD + GCM was adopted; the same model was applied to investigate the ND and SD bands of ^{40}Ca in Ref. [24]. We also investigated the ND and SD states of $^{41}_{\Lambda}$Ca, $^{46}_{\Lambda}$Sc, and $^{48}_{\Lambda}$Sc using the HyperAMD. As the effective interactions, the Gogny D1S was adopted for the NN sector, and the latest version of the ESC08c ΛN potential was employed. Major points to be emphasized are as follows:

(i) In ^{40}Ca, we obtained three 0^+ states corresponding to the observed spherical ground, ND, and SD states, which are identical to those reported in Ref. [24]. By addition of a Λ particle to these states, it was found that the calculated Λ-separation energy B_Λ was depending on the degree of deformations: $B_\Lambda = 19.45$ MeV for the ground state $(1/2^+_1)$, $B_\Lambda = 19.15$ MeV for the ND state $(1/2^+_2)$, and $B_\Lambda = 18.01$ MeV for the SD state $(1/2^+_3)$ in $^{41}_{\Lambda}$Ca.

(ii) In the core nuclei ^{45}Sc and ^{47}Sc, we obtained many excited states with different (β,γ) deformations, which have mp-mh configurations. Among these states, we predicted for the first time that ^{45}Sc had SD states in which protons had the same configuration as the SD states of ^{40}Ca. By addition of a Λ particle, the resultant hypernuclei $^{46}_{\Lambda}$Sc and $^{48}_{\Lambda}$Sc had mp-mh states with a Λ in an s orbit. Furthermore, we found that the calculated B_Λ also depended on the degree of deformation: for example, in $^{46}_{\Lambda}$Sc, B_Λ in the SD state was 19.52 MeV, while $B_\Lambda = 19.95$ MeV in the ground state.

(iii) We focused on the level structure of $7/2^-_1$ and $3/2^+_1$ states in ^{45}Sc and ^{47}Sc; these two states were close to each other. Since the deformation β of each state was different, the calculated B_Λ was different from each other. As a result, the corresponding states (1^+_1 and 2^+_1) in $^{46}_{\Lambda}$Sc and $^{48}_{\Lambda}$Sc were shifted up with respect to the 3^-_1 and 4^-_1 states.

TABLE VI. Same as Table V but for the SLS and ALS parts.

β_i	0.4	0.8	1.2
		SLS	
a_i	−11470.0	299.3	−2.386
b_i	21880.0	−744.1	0.0
c_i	−8962.0	294.4	0.0
		ALS	
a_i	2084.0	9.536	1.851
b_i	−1549.0	32.55	0.0
c_i	578.1	−14.52	0.0

To see the above interesting phenomena in $^{46}_{\Lambda}$Sc and $^{48}_{\Lambda}$Sc, we hope to perform high-resolution experiments, ^{46}Ti$(e,e'K^+)^{46}_{\Lambda}$Sc and ^{48}Ti$(e,e'K^+)^{48}_{\Lambda}$Sc at JLab in the future.

ACKNOWLEDGMENTS

The authors would like to thank Professor S. N. Nakamura, Dr. Y. Fujii, Dr. K. Tsukada, and Mr. T. Gogami for valuable discussions and information on the experimental project at JLab. They are also thankful to Professor E. Ideguchi, Professor T. Motoba, and Professor S.-G. Zhou for helpful discussions and encouragement. This work is supported in part by the Grants-in-Aid for Scientific Research on Innovative Areas from MEXT (Grant No. 2404: 24105008). M.I. is supported by the Special Postdoctoral Researcher Program of RIKEN. The numerical calculations were performed on the HITACHI SR16000 at KEK.

APPENDIX: PARAMETERS OF YNG-ESC08C INTERACTION

As for the YN interaction employed in this paper, we used the YNG interaction derived from ESC08c. The parameters a_i, b_i, c_i, and β_i in Eq. (17) are summarized in Tables V and VI for the central, symmetric spin-orbit (SLS), and anti-symmetric spin-orbit (ALS) parts of the G-matrix interaction, respectively.

[1] T. Motoba, H. Bandō, and K. Ikeda, Prog. Theor. Phys. **70**, 189 (1983).

[2] T. Motoba, H. Bandō, K. Ikeda, and T. Yamada, Prog. Theor. Phys. Suppl. **81**, 42 (1985).

[3] E. Hiyama, M. Kamimura, K. Miyazaki, and T. Motoba, Phys. Rev. C **59**, 2351 (1999).
[4] E. Hiyama, M. Kamimura, T. Motoba, T. Yamada, and Y. Yamamoto, Prog. Theor. Phys. **97**, 881 (1997).
[5] E. Hiyama, M. Kamimura, T. Motoba, T. Yamada, and Y. Yamamoto, Phys. Rev. Lett. **85**, 270 (2000).
[6] M. Isaka, M. Kimura, A. Doté, and A. Ohnishi, Phys. Rev. C **83**, 044323 (2011).
[7] T. Sakuda and H. Bandō, Prog. Theor. Phys. **78**, 1317 (1987).
[8] T. Yamada, K. Ikeda, H. Bandō, and T. Motoba, Prog. Theor. Phys. **71**, 985 (1984).
[9] M. Isaka, M. Kimura, A. Doté, and A. Ohnishi, Phys. Rev. C **83**, 054304 (2011).
[10] M. T. Win and K. Hagino, Phys. Rev. C **78**, 054311 (2008).
[11] J. Kownacki, L. Harms-Ringdahl, J. Sztarkier, and Z. Sawa, Phys. Scr. **8**, 135 (1973).
[12] P. Bizzeti, A. Bizzeti-Sona, M. Bucciolini, R. Huber, W. Kutschera, H. Morinaga, R. Ricci, and C. Signorini, Nuovo Cimento A **26**, 25 (1975).
[13] J. Styczen, J. Chevallier, B. Haas, N. Schulz, P. Taras, and M. Toulemonde, Nucl. Phys. A **262**, 317 (1976).
[14] D. Avasthi, K. Jain, I. Govil, and V. Mittal, Act. Phys. Pol. B **16**, 847 (1985).
[15] M. T. Win, K. Hagino, and T. Koike, Phys. Rev. C **83**, 014301 (2011).
[16] B.-N. Lu, E.-G. Zhao, and S.-G. Zhou, Phys. Rev. C **84**, 014328 (2011).
[17] E. Hiyama and Y. Yamamoto, Prog. Theor. Phys. **128**, 105 (2012).
[18] C. E. Svensson, A. O. Macchiavelli, A. Juodagalvis, A. Poves, I. Ragnarsson, S. Aberg, D. E. Appelbe, R. A. E. Austin, C. Baktash, G. C. Ball *et al*., Phys. Rev. Lett. **85**, 2693 (2000).
[19] E. Ideguchi, D. G. Sarantites, W. Reviol, A. V. Afanasjev, M. Devlin, C. Baktash, R. V. F. Janssens, D. Rudolph, A. Axelsson, M. P. Carpenter *et al*., Phys. Rev. Lett. **87**, 222501 (2001).
[20] C. D. O'Leary, M. A. Bentley, B. A. Brown, D. E. Appelbe, R. A. Bark, D. M. Cullen, S. Ertürk, A. Maj, and A. C. Merchant, Phys. Rev. C **61**, 064314 (2000).
[21] J. R. MacDonald, D. H. Wilkinson, and D. E. Alburger, Phys. Rev. C **3**, 219 (1971).
[22] E. Ideguchi, S. Go, H. Miya, K. Kisamori, M. Takaki, R. Yokoyama, T. Fujii, S. Ota, S. Michimasa, S. Shimoura *et al*., N-SI-49 ORGAM, experimental proposal submitted to GANIL.
[23] Y. Kanada-En'yo and M. Kimura, Phys. Rev. C **72**, 064322 (2005).
[24] Y. Taniguchi, M. Kimura, Y. Kanada-En'yo, and H. Horiuchi, Phys. Rev. C **76**, 044317 (2007).
[25] T. Rijken, M. Nagels, and Y. Yamamoto, Prog. Theor. Phys. Suppl. **185**, 14 (2010).
[26] Y. Yamamoto, T. Motoba, and T. Rijken, Prog. Theor. Phys. Suppl. **185**, 72 (2010).
[27] J. Dechargé and D. Gogny, Phys. Rev. C **21**, 1568 (1980).
[28] M. Kimura, Phys. Rev. C **75**, 034312 (2007).
[29] M. Kimura and N. Furutachi, Phys. Rev. C **83**, 044304 (2011).
[30] T. Rijken, M. Nagels, and Y. Yamamoto (unpublished).
[31] W. Gerace and A. Green, Nucl. Phys. A **93**, 110 (1967).
[32] W. Gerace and A. Green, Nucl. Phys. A **123**, 241 (1969).
[33] A. Gal, Adv. Nucl. Phys. **8**, 1 (1975).
[34] B. H. Flowers and I. P. Johnstone, Proc. Phys. Soc., London **91**, 310 (1967).
[35] I. Johnstone, Nucl. Phys. A **110**, 429 (1968).
[36] J. S. Forster, G. C. Ball, F. Ingebretsen, and C. F. Monahan, Phys. Lett. B **32**, 451 (1970).
[37] G. C. Ball, J. S. Forster, D. Ward, and C. F. Monahan, Phys. Lett. B **37**, 366 (1971).
[38] P. Bednarczyk, J. Styczen, R. Broda, M. Lach, W. Meczynski, D. Bazzacco, F. Brandolini, G. Angelis, S. Lunardi, L. Muller *et al*., Eur. Phys. J. A **2**, 157 (1998).
[39] N. Stone, At. Data Nucl. Data Tables **90**, 75 (2005).
[40] M. Avgoulea, Y. P. Gangrsky, K. P. Marinova, S. G. Zemlyanoi, S. Fritzsche, D. Iablonskyi, C. Barbieri, E. C. Simpson, P. D. Stevenson, J. Billowes *et al*., J. Phys. G **38**, 025104 (2011).